ACS APPLIED MATERIALS & INTERFACES

Research Article

www.acsami.org

Synthesis of $Na_{1.25}V_3O_8$ Nanobelts with Excellent Long-Term Stability for Rechargeable Lithium-Ion Batteries

Shuquan Liang,[†] Tao Chen,[†] Anqiang Pan,*[,†] Dawei Liu,[‡] Qinyu Zhu,[†] and Guozhong Cao*[,§]

[†]School of Materials Science & Engineering, Central South University, Changsha, Hunan 410083, China

[‡]Department of Materials Science & Engineering, Kazuo Inamori School of Engineering, New York State College of Ceramics, Alfred University, Alfred, New York 14802, United States

[§]Department of Materials Science & Engineering, University of Washington, Seattle, Washington 98195, United States

ABSTRACT: Sodium vanadium oxide ($Na_{1.25}V_3O_8$) nanobelts have been successfully prepared by a facile sol–gel route with subsequent calcination. The morphologies and the crystallinity of the as-prepared $Na_{1.25}V_3O_8$ nanobelts can be easily controlled by the calcination temperatures. As cathode materials for lithium ion batteries, the $Na_{1.25}V_3O_8$ nanobelts synthesized at 400 °C exhibit a relatively high specific discharge capacity of 225 mA h g^{-1} and excellent stability at 100 mA g^{-1}. The nanobelt-structured electrode can retain 94% of the initial capacity even after 450 cycles at the current density of 200 mA g^{-1}. The good electrochemical performance is attributed to their nanosized thickness and good crystallinity. The superior electrochemical performance demonstrates the $Na_{1.25}V_3O_8$ nanobelts are promising cathode materials for secondary lithium batteries.

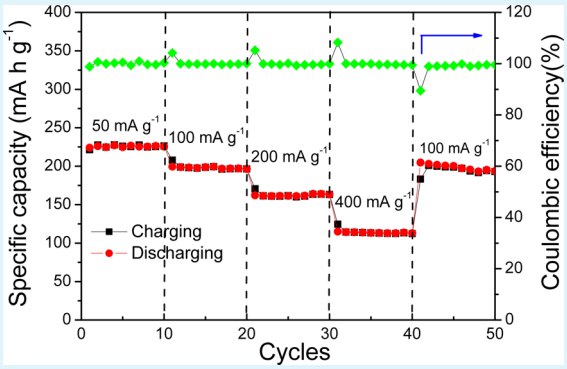

KEYWORDS: *sodium vanadium oxide, nanobelts, sol–gel, lithium-ion batteries, long-term stability*

1. INTRODUCTION

Because of their high energy density, long life cycle, environmentally benign, lithium ion batteries (LIBs) have been widely used in portable electronic devices. They are also under serious consideration to power HEVs and EVs, which require higher energy densities and power capability.[1,2] The state-of-the-art $LiCoO_2$ cathode material has a specific discharge capacity of ~140 mA h g^{-1} and the widely studied $LiFePO_4$ has a theoretical capacity of 170 mA h g^{-1}.[2,3] Therefore, it is urgent to develop alternative cathode materials with higher capacity and energy density to satisfy the customers' increasing demand.[4,5]

Lithium trivanadate ($Li_{1+x}V_3O_8$) has been extensively studied as a cathode material for lithium-ion batteries in the last decades because of its good structural reversibility and high capacity.[6−8] A theoretical capacity of 372.5 mA h g^{-1} can be reached when four Li^+ ions are successfully intercalated per formula of LiV_3O_8.[9−11] Pan et al. have reported the preparation of nanosheet-structured LiV_3O_8 and their superior cycling stability as a cathode material for LIBs.[12] However, the rate performance still needs further improvement. Recently, other cations with larger ionic radius, such as NH_4^+ and Na^+, are also incorporated into the $(V_3O_8)^-$ layers to obtain good cyclic stability.[13,14] Sodium vanadium oxide ($Na_{1+x}V_3O_8$), with isostructure to $Li_{1+x}V_3O_8$, has attracted much attention due to the abundance of Na^+ in storage and more importantly the larger interlayer distance, which potentially can improve the mobility of the Li^+ ions during the lithium ions intercalation/deintercalation process.[15,16] The structure of $Na_{1+x}V_3O_8$ is composed of $(V_3O_8)^-$ layers along *a* axis, pinned together by Na^+ ion at the octahedral sites in the interlayer.[17] Spahr et al. have reported the synthesis of $Li_3NaV_3O_8$ via aqueous precipitation with subsequent chemical lithiation and the good cycling performance of the electrode between 1.5 and 4.0 V.[18] Wang et al. prepared the nanowire-structured $Na_2V_6O_{16}{\cdot}0.86H_2O$, which delivered an initial specific discharge capacity of 235 mA h g^{-1} at 30 mA g^{-1} and remained 91.1% of its original capacity.[14] However, their electrochemical performance, such as long-term stability and rate capability, still needs further improvement.

Nanomaterials have been widely explored in LIBs because of their appealing properties, such as reduced Li^+ ions diffusion and electron transportation distance, enlarged contact area between electrode and electrolyte, and easier accommodation to the stress upon Li^+ ions take-up and removal process.[19−21] To date, $Na_{1+x}V_3O_8$ with various nanostructures, such as nanowires,[14,22] nanosheets,[23] and nanobelts,[17,24] have been successfully reported. Wang et al. reported the hydrothermal preparation of $Na_{1+x}V_3O_8$ nanowires and nanosheets and demonstrated both the morphology and the crystallinity of the $Na_{1+x}V_3O_8$ had a great effect to their electrochemical performance.[14,23] However, so far, the $Na_{1+x}V_3O_8$ are predominantly prepared by the hydrothermal method, and a subsequent calcination process is commonly required in order

Received: August 27, 2013
Accepted: October 22, 2013
Published: October 22, 2013

to get $Na_{1+x}V_3O_8$ with good crystallinity. It is of great interest to the scientific community to develop a new synthesis strategy that can produce nanostructured $Na_{1+x}V_3O_8$ with high crystallinity in large scale.

Herein, we reported the facile synthesis of $Na_{1.25}V_3O_8$ nanobelts by a sol−gel route with subsequent calcination in air. As cathode materials for LIBs, they deliver high capacity and exhibit excellent long-term stability. The relationship between the superior electrochemical performance and the electrode morphologies/crystallinities will also be discussed.

2. EXPERIMENTAL SECTION

All chemicals were of analytical grade and were used as received without further purification. V_2O_5 (1.2 g) and oxalic acid in a molar ratio of 1:3 were added into a beaker containing 40 mL of deionized (DI) water and magnetically stirred at room temperature until the formation of a clear blue solution, indicating the formation of vanadium oxalate.[20] The reaction can be expressed as follows:

$$V_2O_5 + 3H_2C_2O_4 \rightarrow 2VOC_2O_4 + 2CO_2 + 3H_2O \quad (1)$$

Then, a stoichiometric amount of sodium nitrate ($NaNO_3$) was subsequently added into the preprepared VOC_2O_4 solution under stirring for 1 h. The mixture solution was dried at 80 °C before respective calcination at 350, 400, and 450 °C in air for 8 h. The obtained materials were designated as Na350, Na400, and Na450, respectively. $Na_{1.25}V_3O_8$ bulk material was also prepared by a conventional solid-state method from the mixture of V_2O_5 and $NaNO_3$ in air at 630 °C for 8 h. The obtained product was designated as NaHT.

The calcination process in air was studied by thermogravimetric analysis (TGA) and differential scanning calorimetry (DSC) using a heating rate of 10 °C min^{-1}. The crystallinity and phases of the as-prepared samples were examined by X-ray diffraction (XRD, Rigaku D/max2500 XRD with Cu Kα radiation, λ = 1.54178 Å) with a scan rate of 10° s^{-1} between 10° and 70°. The scanning electron microscopy (SEM, FEI Sirion200) was used to characterize the morphologies of the prepared products.

The samples were assembled into coin cells for electrochemical performance measurements. The $Na_{1.25}V_3O_8$, acetylene black, and polyvinylidene fluoride in a weight ratio of 70:20:10 were made into cathode materials. The Li/$Na_{1.25}V_3O_8$ cells (2016 type coin cells) were assembled in a glovebox (Mbraun, Germany) filled with ultrahigh purity argon using polypropylene membrane as the separator and 1-M $LiPF_6$ in ethylene carbonate/dimethyl carbonate (EC/DMC) (1:1 v/v) as the electrolyte. The cyclic voltammetry (CV) measurement was conducted on CHI660C (CH Instrument Electrochemical workstation), and the galvanostatic discharging/charging experiment was tested on a Land Battery Tester (Land CT 2001A, Wuhan, China). The measurements are all carried out in the voltage range of 1.5−4.0 V (vs Li/Li^+).

3. RESULTS AND DISCUSSION

Figure 1a shows the TG and DSC results of the precursor mixture calcined in air using a ramping rate of 10 °C min^{-1}. Three discrete regions have been observed on the TG curve. The first weight-loss below 250 °C is mainly ascribed to the evaporation of the physically absorbed and chemically bonded water in the precursor.[6] The dramatic weight loss on TG curve thereafter and the corresponding exothermal peaks around 300 °C on the DSC curve indicate the decomposition of the precursor mixture, the removal of organic components, and the release of heat in this temperature range. The followed slight weight increase after 360 °C can be attributed to the trapping of oxygen through the further oxidation of vanadium species. The sharp endothermic peak at 580 °C suggests the materials start to melt.

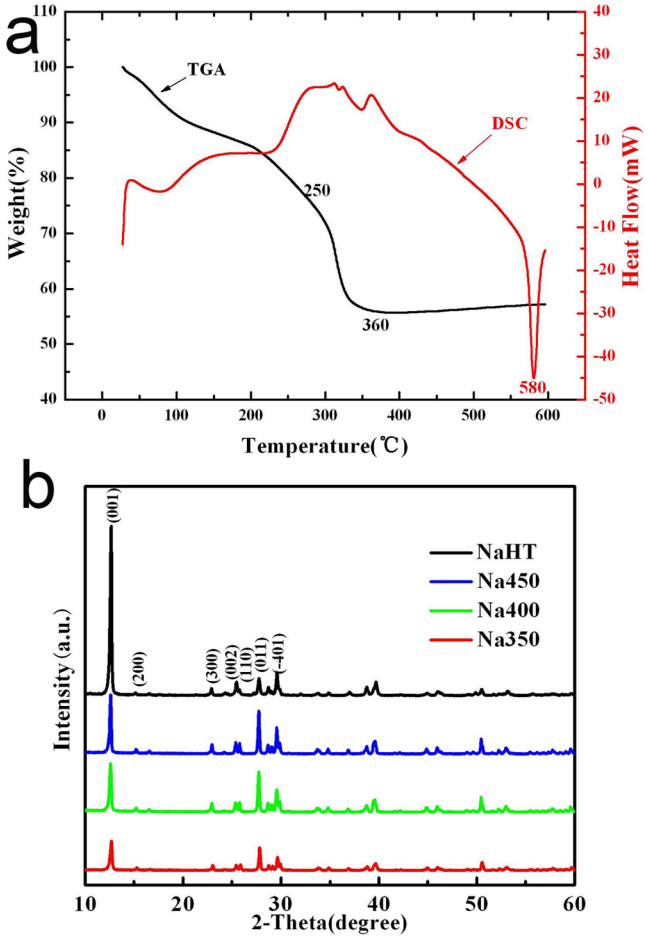

Figure 1. (a) TG and DSC results of the calcinating process in air for the dried solids ($NaNO_3$ and VOC_2O_4) from 25 to 600 °C. The heating rate was 10 °C min^{-1}. (b) XRD patterns for calcination products of Na350, Na400, Na450, and NaHT.

The crystallinity and phases of the products prepared by the high-temperature solid-state approach and the sol−gel route were characterized by XRD, and the results are shown in Figure 1b. The main diffraction peaks have been indexed, and the XRD patterns can be well assigned to $Na_{1.25}V_3O_8$ phase (space group: $P2_1/m$ (11), JCPDS card 24-1156, a = 12.140, b = 3.612, c = 7.320). No detection of other phases indicates the high purity of the prepared products. Moreover, the intensities of the peaks increase with the raise of the calcination temperatures. The result demonstrates the precursor mixture has been readily converted to $Na_{1.25}V_3O_8$ at 350 °C. The NaHT material has a sharper peak of (001) plane and higher intensity than the samples prepared by the sol−gel route. The result indicates the crystallites of the conventional solid-state method prepared $Na_{1.25}V_3O_8$ are much larger, which would probably limit their kinetics for Li^+ ions intercalation. The sodium vanadium oxides synthesized at lower temperatures by the sol−gel assisted route are more favorable to get smaller crystallites.

Figure 2 shows the SEM images of the Na350, Na400, Na450, and NaHT samples. As shown in Figure 2a, typical nanobelts are clearly observed for the Na350 samples with a thickness around 80 nm and a length up to several micrometers. Figure 2b shows the SEM image of the Na400 product, which manifests the $Na_{1.25}V_3O_8$ nanobelts are more uniformly fabricated with similar size. However, the nanobelts

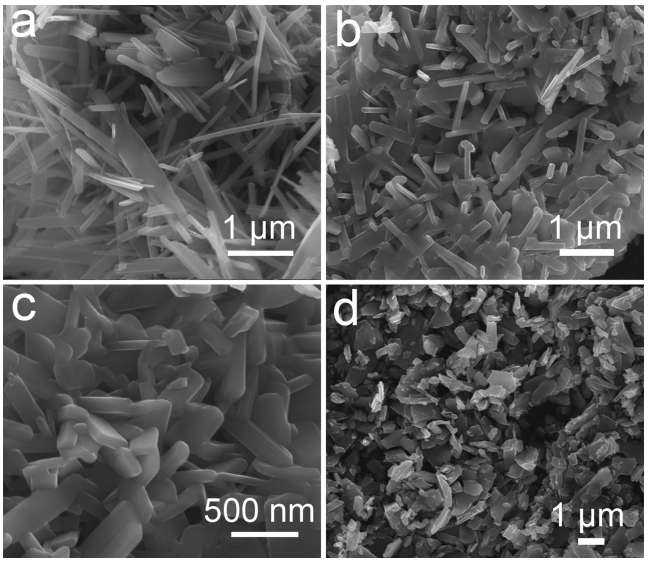

Figure 2. SEM images of Na350 (a), Na400 (b), Na450 (c), and NaHT (d).

become a little bit thicker with a mean size of 100 nm and a length of about 1 μm. The nanobelts become even thicker with a size of 125 nm and start to aggregate for the Na450 sample (see Figure 2c). It is worth noting that the thickness of the prepared nanobelts increases with calcination temperatures. At higher temperatures, the surface and/or bulk diffusivity would increase and thus allow the crystals to achieve or get closer to their thermodynamic equilibrium shape. The nanobelts may not be the most favorable morphology (not with the lowest total surface energy). Similar results have been reported on LiV_3O_8 nanorods in our previous works.[6] Figure 2d shows the morphology of the NaHT sample obtained at 630 °C, which reveals the particles are much larger and more densely compacted. Most of the particles are of micrometer in size and with a thickness of around 500 nm.

Figure 3 shows the first three continuous CV curves for the electrodes tested in the voltage range of 1.5−4.0 V (vs Li/Li^+) with a scan rate of 0.1 mV s^{-1}. As shown in Figure 3a, four cathodic peaks at 3.62, 3.10, 2.41, and 2.18 V are observed, which indicate the multistep lithium ions intercalation process. During the anodic scan, a broad peak at 2.68 V is detected. Although the peak position for Na350 electrode is quite similar, the intensity for the first three consecutive cycles decreases gradually (see Figure 3a). However, the CV curves are largely overlapped for Na400 electrode, suggesting the good reversibility of the lithium ions interaction/deintercalation process and the good retention of crystallinity (see Figure 3b). As shown in Figure 3c, the intensities of the CV curves of NaHT electrode increase continuously, which indicate the activation of the electrode by the electrochemical grinding.

Figure 4 shows the cyclic performance of Na400 and NaHT electrodes at the current density of 100 mA g^{-1} in the voltage range of 1.5−4 V vs Li/Li^+. As shown in Figure 4, an initial specific discharge capacity of 191 mA h g^{-1} can be achieved for N400 electrode, which increases slightly to a maximum discharge capacity of 225 mA h g^{-1} at the 44th cycle. After 70 cycles, it still retains a specific discharge capacity of 217 mA h g^{-1}, showing promising capacity retention. The NaHT electrode only releases an initial discharge capacity of 49 mA h g^{-1} and increases continuously to 73 mA h g^{-1} after 70 cycles.

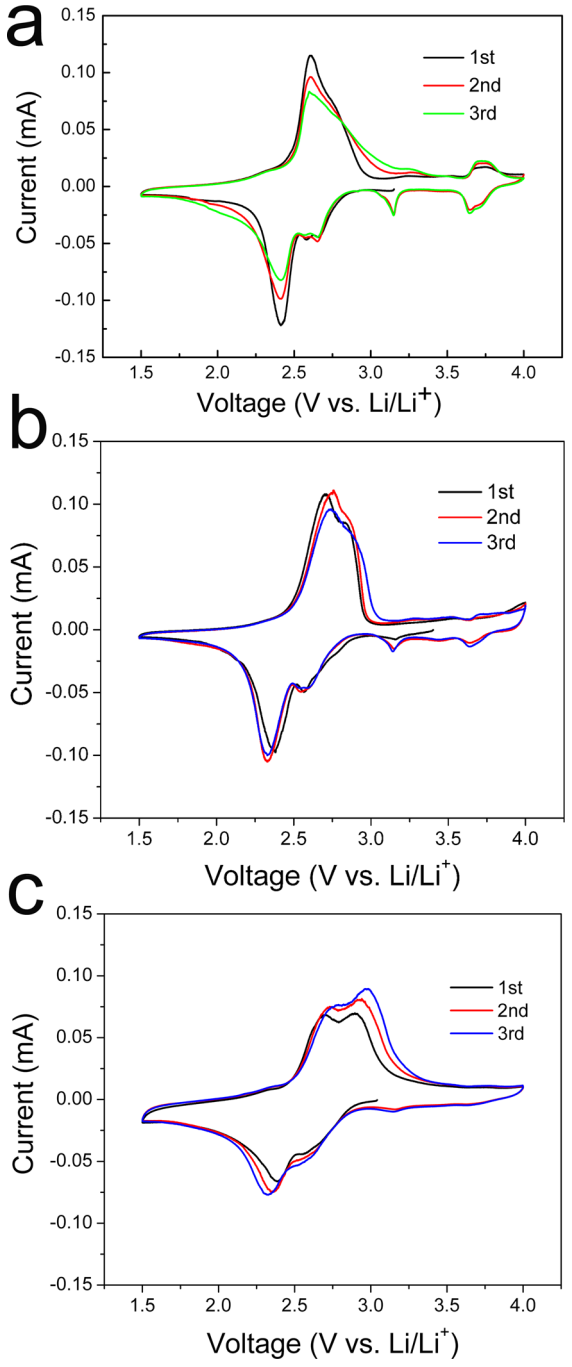

Figure 3. The first three consecutive cyclic voltammetry (CV) curves for Na350 (a), Na400 (b), and NaHT (c) electrodes at a scan rate of 0.1 mV s^{-1}.

The cycling performance of NaHT electrode corresponds well with its CV curves (see Figure 3c), and the capacity increase can be attributed to the electrochemical activation process for NaHT electrode. The particle size of NaHT material is of micrometers, which may be broken into smaller pieces during electrochemical cycling. Thus, the thermodynamic for the lithium ion intercalation/deintercalation can be improved. However, the electrochemical properties of NaHT electrode are still inferior to Na400 electrode because the size of the larger particle size of NaHT.

Figure 5 shows the cycling performance of the Na350, Na400, and Na450 electrodes at the current density of 100 mA

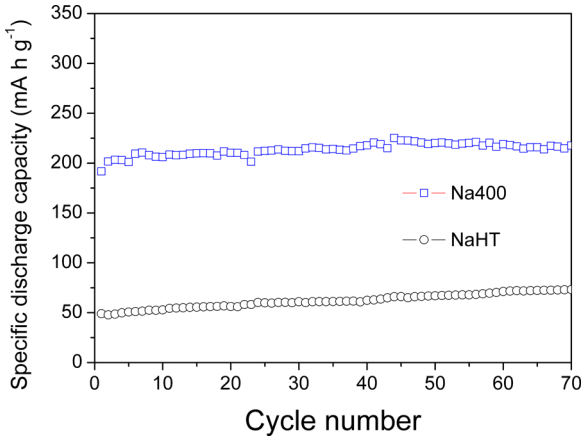

Figure 4. The cycling performance of Na400 and NaHT electrodes in the voltage range of 1.5−4.0 V (vs Li/Li^+) under a current density of 100 mA g^{-1}.

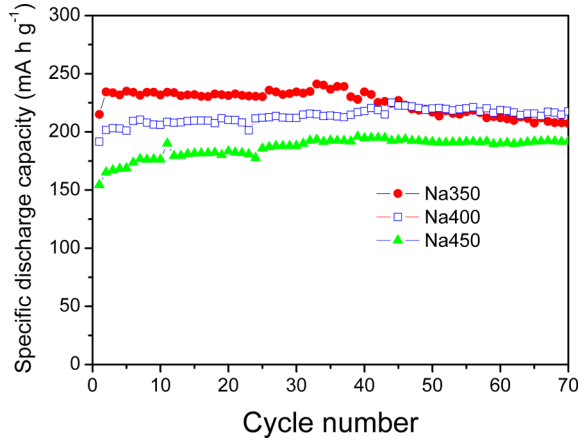

Figure 5. The cycling performance of Na350, Na400, and Na450 electrodes in the voltage range of 1.5−4.0 V (vs Li/Li^+) at a current density of 100 mA g^{-1}.

g^{-1}. The Na350, Na400, and Na450 electrodes deliver the initial discharge capacities of 215, 192, and 154 mA h g^{-1}, respectively, and their maximum discharge capacities of 241, 225, and 195 mA h g^{-1}, correspondingly. The higher specific discharge capacity detected for Na350 electrode than the other two electrodes can be ascribed to the smaller thickness of the nanobelts (80 nm) and larger space between the nanobelts (shown in Figure 2). Higher annealing temperature leads to larger-sized crystallites and lower surface energy, which is thermodynamically unfavorable to get higher discharge capacity. However, the capacity of Na350 electrode starts to degrade after 40 cycles and remains a specific discharge capacity of 207 mA h g^{-1} at 70th cycle, the cycling stability of which is not as good as those for the Na400 and Na450 electrodes. It is believed that sodium vanadates with higher crystallinity can have better structural stability during cycling. Similar phenomenon has been reported for $Na_2V_6O_{16}{\cdot}xH_2O$ nanowires[14] and NaV_6O_{15} nanorods.[25] There should be a balance between particle size and crystallinity in order to get superior electrochemical performance. In our case, the Na400 electrode fabricated at 400 °C has the best comprehensive performance with relatively high capacity and good cycling stability.

Figure 6 shows the rate capability of the Na400 electrode at various current densities. A specific discharge capacity of 225

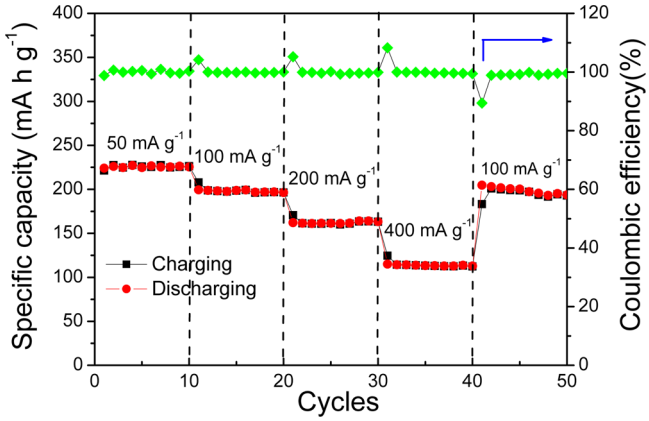

Figure 6. The rate performance of Na400 electrode in the voltage range of 1.5−4.0 V (vs Li/Li^+).

mA h g^{-1} can be obtained for Na400 electrode at the current density of 50 mA g^{-1}, and it can deliver the specific discharge capacities of 199, 162, and 115 mA h g^{-1} at the current density of 100, 200, and 400 mA g^{-1}, respectively. When the current was reset to 100 mA g^{-1}, a specific discharge capacity of 203 mA h g^{-1} can be recovered. As shown in Figure 6, the electrode shows good cyclic stability at various current densities. Moreover, the Coulombic efficiency is close to 100%, which indicates the good reversibility of the electrodes. The superior electrochemical performance can be attributed to the novel nanobelts and the good crystallinity of the Na400 electrode. The nanobelts are thermodynamically favorable for lithium ions intercalation/deintercaltion, and the good crystallinity can ensure the structural stability upon cycling.

Figure 7 shows the long-term cycling performance and the corresponding Coulombic efficiency of Na400 electrode at the current density of 200 mA g^{-1}. An initial discharge capacity of 172 mA h g^{-1} can be delivered, and it increases slightly to reach a maximum capacity of 187 mA h g^{-1} at the 45th cycle. As shown in Figure 7a, the discharge curves of the 1st, 100th, 250th, and 450th cycles are quite similar, which suggest the good structural reversibility upon cycling. The plateaus shown on the charge curves shift to higher voltage and become more obvious, which can be ascribed to the polarization after long-term cycling. However, the Na400 electrode still retains a specific discharge capacity of 164 mA h g^{-1} after 450 cycles with a capacity retention of 94%. The Coulombic efficiency is close to 100% and remains very stable upon cycling (see Figure 7b). The cyclic stability is much better than other vanadium-based cathode materials, such as V_2O_5,[26] LiV_3O_8,[6] NaV_3O_8,[14] and $Na_{0.33}V_2O_5$.[25,27] It is even better than their carbon composites, such as V_2O_5/CNT[28,29] and V_2O_5/graphene composites.[30] The excellent long-term cyclic stability can be attributed to the nanobelt-structured $Na_{1.25}V_3O_8$ particles with good crystallinity: (1) the nanosized thickness of $Na_{1.25}V_3O_8$ nanobelts can shorten the Li^+ ions diffusion and electron transportation distance; (2) the empty space between neighboring nanobelts can allow electrolyte penetration, thus improving the wettability of the electrodes; (3) the high purity and good crystallinity can keep the structural integrity during cycling.

4. CONCLUSIONS

In summary, a reliable sol−gel route has been developed to fabricate $Na_{1.25}V_3O_8$ nanobelts. The thickness and the

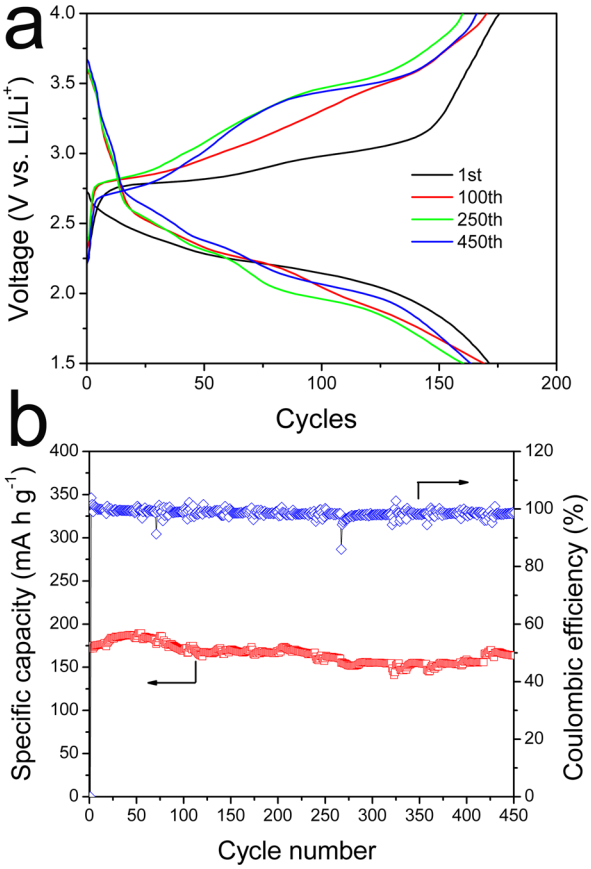

Figure 7. (a) The discharge/charge curves of the 1st, 100th, 250th, and 400th cycles; (b) the cycling performance and Coulombic efficiency of the Na400 electrodes in the voltage range of 1.5−4.0 V (vs Li/Li^+) at a current density of 200 mA g^{-1}.

crystallinity of $Na_{1.25}V_3O_8$ nanobelts increase with the calcination temperatures. As a cathode material for lithium ion batteries, the as-prepared $Na_{1.25}V_3O_8$ nanobelts exhibit much higher capacity than the $Na_5V_{12}O_{32}$ bulk particles synthesized by the conventional high-temperature solid-state method. The electrochemical performances of the $Na_{1.25}V_3O_8$ nanobelts are dependent on their morphologies and crystallinity. The $Na_{1.25}V_3O_8$ nanobelts synthesized at 400 °C shows relatively high specific discharge capacity and excellent stability, which retain 94% of the initial capacity after 450 cycles.

AUTHOR INFORMATION

Corresponding Authors

*E-mail: pananqiang@gmail.com (A. Pan).
*E-mail: gzcao@u.washington.edu (G. Z. Cao).

Notes

The authors declare no competing financial interest.

ACKNOWLEDGMENTS

The financial support is provided by National High-tech R&D Program (863, Grant No. 2013AA110106) and Lie-Ying Program of Central South University.

REFERENCES

(1) Armand, M.; Tarascon, J.-M. *Nature* **2008**, *451*, 652.
(2) Tarascon, J.-M.; Armand, M. *Nature* **2001**, *414*, 359.
(3) Xie, H.-M.; Wang, R.-S.; Ying, J.-R.; Zhang, L.-Y.; Jalbout, A. F.; Yu, H.-Y.; Yang, G.-L.; Pan, X.-M.; Su, Z.-M. *Adv. Mater.* **2006**, *18*, 2609.
(4) Liu, D. W.; Cao, G. Z. *Energy Environ. Sci.* **2010**, *3*, 1218.
(5) Lee, C.-Y.; Marschilok, A. C.; Subramanian, A.; Takeuchi, K. J.; Takeuchi, E. S. *Phys. Chem. Chem. Phys.* **2011**, *13*, 18047.
(6) Pan, A. Q.; Liu, J.; Zhang, J.-G.; Cao, G. Z.; Xu, W.; Nie, Z. M.; Xiao, J.; Choi, D.; Arey, B. W.; Wang, C. M.; Liang, S.-Q. *J. Mater. Chem.* **2011**, *21*, 1153.
(7) Xu, X.; Luo, Y.-Z.; Mai, L.-Q.; Zhao, Y.-L.; An, Q.-Y.; Xu, L.; Hu, F.; Zhang, L.; Zhang, Q.-J. *NPG Asia Mater.* **2012**, *4*, No. e20.
(8) Feng, Y.; Hou, F.; Li, Y. L. *J. Power Sources* **2009**, *192*, 708.
(9) Pistoia, G.; Wang, G.; Zane, D. *Solid State Ionics* **1985**, *76*, 285.
(10) Psaquali, M.; Pistoia, G. *Electrochim. Acta* **1991**, *36*, 1549.
(11) Gu, Y. X.; Chen, D. R.; Jiao, X. L.; Liu, F. F. *J. Mater. Chem.* **2006**, *16*, 4361.
(12) Pan, A. Q.; Zhang, J.-G.; Cao, G. Z.; Liang, S.-Q.; Wang, C. M.; Nie, Z. M.; Arey, B. W.; Xu, W.; Liu, D. W.; Xiao, J.; Li, G. S.; Liu, J. *J. Mater. Chem.* **2011**, *21*, 10077.
(13) Wang, H. Y.; Huang, K. R.; Liu, S. Q.; Huang, C. H.; Wang, W. J.; Ren, Y. *J. Power Sources* **2011**, *196*, 788.
(14) Wang, H.; Wang, W. J.; Ren, Y.; Huang, K. R.; Liu, S. Q. *J. Power Sources* **2012**, *199*, 263.
(15) Kawakita, J.; Miura, T.; Kishi, T. *Solid State Ionics* **1999**, *124*, 21.
(16) Kawakita, J.; Miura, T.; Kishi, T. *Solid State Ionics* **1999**, *124*, 29.
(17) Xue, Y.; Wu, J.; Zhang, H. Y.; Luo, Y.; Zhang, X. D.; Du, Z. L.; Xie, Y. *RSC Adv.* **2012**, *2*, 7290.
(18) Spahr, M. E.; Novak, P.; Scheifele, W.; Haas, O.; Nesper, R. *J. Electrochem. Soc.* **1998**, *145*, 421.
(19) Arico, A. S.; Bruce, P.; Scrosati, B.; Tarascon, J.-M.; Schalkwijk, W. V. *Nat. Mater.* **2005**, *4*, 366.
(20) Pan, A. Q.; Wu, H. B.; Yu, L.; Lou, X. W. *Angew. Chem., Int. Ed.* **2013**, *52*, 2226.
(21) Wang, Y.; Cao, G. Z. *Adv. Mater.* **2008**, *20*, 2251.
(22) Avansi, W., Jr.; Ribeiro, C.; Leite, E. R.; Mastelaro, V. R. *Mater. Chem. Phys.* **2011**, *127*, 56.
(23) Wang, H.; Liu, S. Q.; Ren, Y.; Wang, W. J.; Tang, A. D. *Energy Environ. Sci.* **2012**, *5*, 6173.
(24) Yu, J. G.; Yu, J. C.; Ho, W. K.; Wu, L.; Wang, X. C. *J. Am. Chem. Soc.* **2004**, *126*, 3422.
(25) Liu, H. M.; Wang, Y. G.; Li, L.; Wang, K. X.; Hosono, E.; Zhou, H. S. *J. Mater. Chem.* **2009**, *19*, 7885.
(26) Mai, L.-Q.; Xu, L.; Han, C. H.; Xu, X.; Luo, Y. Z.; Zhao, S. Y.; Zhao, Y. L. *Nano Lett.* **2010**, *10*, 4750.
(27) Baddour-Hadjean, R.; Bach, S.; Emery, N.; Pereira-Ramos, J. P. *J. Mater. Chem.* **2011**, *21*, 11296.
(28) Sathiya, M.; Prakash, A. S.; Ramesh, K.; Tarascon, J.-M.; Shukla, A. K. *J. Am. Chem. Soc.* **2011**, *133*, 16291.
(29) Jia, X. L.; Chen, Z.; Suwarnasarn, A.; Rice, L.; Wang, X. L.; Sohn, H.; Zhang, Q.; Wu, B. M.; Wei, F.; Lu, Y. F. *Energy Environ. Sci.* **2012**, *5*, 6845.
(30) Liu, H. M.; Yang, W. S. *Energy Environ. Sci.* **2011**, *4*, 4000.